Estimating the impact of the cryptic degassing of Large Igneous Provinces: A mid-Miocene case-study

David I. Armstrong M^{c}Kay*[1], Toby Tyrrell[1], Paul A. Wilson[1] & Gavin L. Foster[1]

[1] **National Oceanography Centre Southampton, University of Southampton, Southampton, SO14 3ZH, UK**

*** D.Armstrong-McKay@noc.soton.ac.uk**

Published in Earth and Planetary Science Letters:

Armstrong McKay, D.I., Tyrrell, T., Wilson, P.A., Foster, G.L., 2014. Estimating the impact of the cryptic degassing of Large Igneous Provinces: A mid-Miocene case-study. Earth Planet. Sci. Lett. 403, 254–262.

Version of Record available at: http://dx.doi.org/10.1016/j.epsl.2014.06.040

Abstract

Large Igneous Provinces (LIPs) have been emplaced throughout Earth's history, erupting great quantities (>10^4 km^3) of lava in long-lived (>10^5 y) events that have been linked to major environmental disruptions. The largest LIP eruptions (e.g. Siberian Traps) are widely considered to have had an impact on global climate through basalt CO_2 degassing but the impact of the more numerous smaller LIPs is debated. Here we test the hypothesis that LIPs had a greater impact on Earth's climate history than previously estimated because of the 'cryptic degassing' of intruded and crust-contaminated magma, injecting extra CO_2 over and above that coming from sub-aerial basalts. We use biogeochemical box models to investigate the potential impact of the Columbia River Basalts (CRB) during the mid-Miocene where multiple palaeorecords for this geologically relatively recent event enable more rigorous data-model comparison. We find that the effect on the long-term carbon cycle of basalt degassing from the CRB alone is negligible, but that a total CRB emission of 4090-5670 Pg of carbon with 3000-4000 Pg of this carbon emitted during the Grande Ronde Basalt eruptions, a flux within the acceptable estimated range when cryptic degassing is included, does well in reproducing the record of benthic $\delta^{13}C$ and atmospheric CO_2 change during the core of the Miocene Climatic Optimum. Nevertheless, mechanisms other than degassing are required to drive observed warmth before 16.3 Ma and to match observed calcite compensation depth behaviour after ~15.4 Ma. Hence, our findings rule out the possibility that CRB emplacement alone can fully explain the mid-Miocene record but they demonstrate the enhanced climate impact that occurs when substantial cryptic degassing accompanies LIP emplacement.

Keywords: Mid-Miocene, Columbia River Basalt, Large Igneous Province, Cryptic Degassing, Climate change, Volcanic degassing

1. Introduction

Large Igneous Provinces (LIPs) erupt great quantities of lava during long-lived events that can release significant volumes of carbon into the ocean-atmosphere system (Bryan and Ernst, 2008; Coffin and Eldholm, 1994; Courtillot and Renne, 2003; Ernst et al., 2005). While the LIPs with the largest volumes (e.g. the Siberian Traps or the Central Atlantic Magmatic Province) are widely accepted to have triggered episodes of carbon cycle perturbation, global warmth and ecological crisis (Grard et al., 2005; Sobolev et al., 2011; Wignall, 2005, 2001), the case for LIPs with smaller ($\leq 2 \times 10^6$ km^3) volumes (e.g., the Deccan Traps or the Columbia River Basalt), emitting sufficient CO_2 to cause a significant global impact is a subject of debate (Caldeira and Rampino, 1990; Diester-Haass et al., 2009; Kender et al., 2009; Self et al., 2006; Taylor and Lasaga, 1999). However, estimates of LIP CO_2 emissions often do not take into account all of the potential sources of excess or 'cryptic' degassing, which include the often extensive volume of intrusive magma emplaced beneath LIPs (Grard et al., 2005; Karlstrom and Richards, 2011; Menand and Phillips, 2007; Shinohara, 2008), the metamorphic degassing of carbon-rich country rocks (Aarnes et al., 2011a; Erwin, 2006; Ganino and Arndt, 2010, 2009; Iacono-Marziano et al., 2012; Retallack and Jahren, 2008; Svensen et al., 2009, 2004), and the potential impact of the recycling of mafic crust into the LIP magma source (Sobolev et al., 2011). These considerations imply that, under favourable circumstances, many LIPs may have a greater climatic impact than is widely accepted. Here we present the results of a feasibility study to quantify the potential additional impact on the long-term carbon cycle and climate of cryptic degassing using the mid-Miocene Columbia River Basalt (CRB) event for which multiple high-resolution palaeorecords are available.

2. The mid-Miocene and the Columbia River Basalt eruptions

Published composite records of benthic stable isotope and $CaCO_3$ accumulation presented in Figure 1 indicate broadly contemporaneous anomalies (calcite compensation depth (CCD) shoaling, benthic $\delta^{13}C$ maximum, benthic $\delta^{18}O$ minimum, ice sheet extent minimum) in the long-term carbon cycle and climate system during the early to middle Miocene, including the Monterey Carbon Isotope Excursion (MCIE) and Miocene Climatic Optimum (MCO) (Billups and Schrag, 2003; Pälike et al., 2012; Passchier et al., 2011; Vincent and Berger, 1985; Zachos et al., 2008). These marked perturbations occurred at about the same time as the onset of the emplacement of the bulk of the CRB in the Cascadia region of North America over multiple eruption phases between ~16.8 and 15.0 Ma (Baksi, 2013; Barry et al., 2013, 2010; Hooper, 1997, 1988; Reidel et al., 2013b; Wolff and Ramos, 2013) (Fig. 2), with the initiation of the CRB eruptions coinciding with the core of both the MCO and the MCIE (Fig. 1). In detail, the peak of the carbon cycle perturbation occurs ca. 16.0 Ma (Fig. 3), coinciding with the eruption, between 16.3 and 15.9 Ma, of the ~152,000 km^3 Grande Ronde Basalt (GRB) formation over ~400 ky (responsible for ~70% of the CRB; Fig. 2; Barry et al., 2013; Reidel and Tolan, 2013; Reidel et al., 2013b; Wolff and Ramos, 2013). Using a Gaussian filter to remove signals below 420 ky in the benthic foraminifera $\delta^{13}C$ palaeorecord from ODP Site 1146 reveals a + 0.3 ‰ excursion in the secular trend of benthic $\delta^{13}C$ between 16.3 and 15.8 Ma (Fig. 3, panel a) (Holbourn et al., 2007). Atmospheric CO_2 reconstructions feature elevated CO_2 during the MCO, perhaps peaking between 16.3 Ma and 15.8 Ma at 400-500 ppmv despite evidence of increased organic carbon burial during the Monterey Excursion, and then declining by ~13.9 Ma (Fig. 3, panel c) (Foster et al., 2012; Kürschner et al., 2008; Vincent and Berger, 1985; Zhang et al., 2013). The CCD also deepens by ~300 m in the equatorial Pacific at ~16.0 Ma, which has been suggested to represent a recovery from an equatorial "carbonate famine" hypothesised to have caused the CCD to

initially shoal at ~18.0 Ma (Fig. 1; Fig. 3, panel b) (Lyle, 2003; Lyle et al., 2010; Pälike et al., 2012). These correlations have led some authors to invoke CRB activity as the main driver of mid-Miocene climate change (e.g. Hodell and Woodruff, 1994; Kender et al., 2009; Foster et al., 2012). Others have concluded that CRB emissions had a negligible impact on atmospheric CO_2 (Taylor and Lasaga, 1999; Diester-Haass et al., 2009).

To investigate the potential importance for Miocene climate of CRB cryptic degassing we use model simulations to determine the magnitude and duration of carbon emissions necessary to reproduce the observed patterns in benthic $\delta^{13}C$, the CCD and atmospheric CO_2 and evaluate the feasibility of these emission scenarios against the range of potential emissions calculated for the CRB.

3. Materials and Methods

3.1. Modelling

We use two biogeochemical box models to simulate the carbon emissions necessary to drive the changes seen in the palaeorecord: i) the model of Merico et al. (2008) (hereafter referred to as MTW08), and ii) the LOSCAR model (Zeebe et al., 2009). MTW08 is an open system model containing all the major fluxes and processes in the carbon, phosphorus and silica cycles, including the carbonate system, air-sea gas exchange, the organic matter pump, CO_2 drawdown by silicate weathering, calcium carbonate formation and cycling and carbon isotopes (Merico et al., 2008). In contrast, LOSCAR (the Long-term Ocean-atmosphere-Sediment CArbon cycle Reservoir model) includes a simplified phosphorous cycle and no silica cycle but includes a sediment component coupled to the ocean-atmosphere routines, allowing the carbonate system to be better represented by including dissolution processes within the sediment column (Zeebe, 2012; Zeebe et al., 2009). LOSCAR also includes

regional boxes for each ocean basin in contrast to the global ocean of MTW08, providing a better comparison to the Pacific-focused palaeorecords used in this study. Both models are limited by low spatial resolution, uncertainties in mid-Miocene estimates for model parameters, and the lack of dynamic ocean, atmosphere and terrestrial biosphere components. Both models are tuned with estimates for mid-Miocene parameters (Tables S1-3) and then perturbed by CRB emission scenarios with varying increases in volcanic baseline emissions above the model baseline. MTW08 is also used to simulate the impacts of fresh basalt weathering through additional inputs of phosphorus and silica, which we estimate are increased by 1.5 and 2.2 % respectively above baseline inputs during the GRB eruptions before declining to 0.1% above baseline over the next 500 ky as the most reactive basalt is weathered away (Taylor and Lasaga, 1999) (Table 1).

3.2. MTW08 sensitivity analyses

After finding an emission scenario that produces the closest match to the palaeorecords we performed various sensitivity analyses in order to judge the sensitivity of our results to our chosen model parameter settings. To establish the impact of the strength of climate-weathering feedbacks on our results the strength of the climate-weathering feedback in MTW08 is varied. CO_2-dependent weathering in MTW08 is formulated as in Walker and Kasting (1992):

$$W_{car} = F_{car} \times \left(pCO_2/pCO_{2(ini)}\right)^{\alpha_c} \quad (1)$$

$$W_{sil} = F_{sil} \times \left(pCO_2/pCO_{2(ini)}\right)^{\alpha_s} \quad (2)$$

where W_{car} and W_{sil} are the current carbonate and silicate weathering rates, F_{car} and F_{sil} are the initial carbonate and silicate weathering flux, $CO_{2(ini)}$ is the initial atmospheric CO_2, α_c is the carbonate weathering exponent and is 1.0 in MTW08 and 0.4 in LOSCAR, and α_s is the silicate weathering exponent and is 0.3 in MTW08 and 0.2 in LOSCAR. By repeating our

best-fit simulations with different carbonate and silicate weathering exponent values we can analyse the sensitivity of our results to the strength of the climate-weathering feedback used in MTW08. The sensitivity of our results to other key parameters in MTW08, including carbonate and silicate weathering, deep ocean mixing, the rain ratio and sediment carbon burial, is also analysed by calculating a sensitivity index using the formula:

$$S = \left| \frac{p(Y' - Y)}{Y(p' - p)} \right| \quad (3)$$

where S is the sensitivity index, p the parameter value, Y the model results for p, and ' denoting the parameter value and model results after the ± 10 % change in p (Haefner, 1996). A sensitivity index value of $S \leq \pm 0.5$ indicates that the variable Y is robust with respect to changes in the parameter p, whereas Y is sensitive to changes in p if $S >> \pm 1$. We also vary the isotopic value of volcanic emissions from the typical value of -4 ‰ (Table S3) in order to analyse the sensitivity of our results to the volcanic carbon $\delta^{13}C$ parameter.

3.3. Eruption chronology

There are several different eruption chronologies proposed for the CRB eruptions based on different dating methods. Data from $^{40}Ar/^{39}Ar$ and K/Ar dating suggests that the GRB erupted between 15.99 ±0.20 Ma and 15.57 ±0.15 Ma (Barry et al., 2013, 2010), but these dates are subject to relatively large errors and the methodology behind these dates has been criticised for potentially underestimating ages (Baksi, 2013; Wolff and Ramos, 2013). Recent re-dating of the geomagnetic polarity time scale and in particular the "Steens reversal" instead indicates the GRB eruption must have started at 16.29 ±0.07 Ma and lasted 400-500 ky (Baksi, 2013; Jarboe et al., 2010; Wolff and Ramos, 2013). The pre-GRB Steens and Imnaha eruptions are estimated to have begun between 16.9 and 16.4 Ma, while the Wanapum eruptions are estimated to have either erupted slowly over 600-800 ky up to as late

as 14.5 Ma or to have been rapidly erupted by as early as 15.78 ± 0.06 Ma (Baksi, 2013; Barry et al., 2013; Jarboe et al., 2010; Wolff and Ramos, 2013). In this study we base our simulated eruptions primarily on the eruption chronology summarised by Wolff and Ramos (2013), with the Steens and Imnaha basalts erupting between 16.8 and 16.3 Ma and the GRB between 16.3 and 15.9 Ma, although we simulate the Wanapum basalts erupting between 15.6 and 15.0 Ma instead of 15.3 to 14.5 Ma (Barry et al., 2013) (Fig. 2, panel b). We also note that cryptic degassing could have begun while magma migrated through the intrusive sill-dike complex prior to surface eruptions, a scenario which has been hypothesised to have occurred up to several hundred thousand years prior to the Siberian Traps eruptions (Sobolev et al., 2011; Wolff and Ramos, 2013; Wolff et al., 2008). This could result in the timing of cryptic degassing differing from that of the basalt eruptions, which means that it is therefore possible that the GRB eruptions could have started as late as 16.0 Ma but its cryptic degassing may still have begun at ~16.3 Ma. In this study we can constrain the timing of significant cryptic degassing from the observed palaeorecord perturbations, but constraining the extrusive eruption chronology is challenging as the impact of these emissions on the palaeorecords is likely to be negligible relative to the impact of cryptic degassing.

3.4. Cryptic degassing estimates

We define cryptic degassing as the emissions from a LIP beyond the degassing of just its sub-aerial basalts and which are therefore more difficult to constrain and often only partially considered when estimating LIP emissions. Our primary method for estimating cryptic degassing is by estimating the release of CO_2 from intrusive, non-erupted magma as well as from sub-aerial basalts. This degassing is calculated by assuming an average basaltic CO_2 content of 0.2-0.5 wt. % and 70-80% degassing efficiency, yielding a minimum of 1.1 Tg C km^{-3} in our low degassing scenario and a maximum of 3.1 Tg C km^{-3} in our high

degassing scenario (Table 2) (Self et al., 2006; Shinohara, 2008). We assume that all of this CO_2 can reach the atmosphere via either surface fissure eruptions, via fracture-fault systems present in the Columbia Basin before the eruption of the CRB or via fracturing around intrusive bodies triggered by devolatilisation-induced overpressure (Aarnes et al., 2012; Reidel et al., 2013a). Sub-aerial emissions are calculated as the degassing from erupted basalts only, intrusive emissions are calculated as the degassing from the intrusive volume associated with the CRB, and total emissions include both sources. In the case of the GRB the extrusive volume is well constrained at ~152,000 km^3 out of a total CRB volume of ~207,000 km^3 (Bryan and Ernst, 2008; Reidel et al., 2013b), while estimates of the intrusive volume associated with the CRB range from an equivalent intrusive to extrusive volume implied by petrologic modelling (Wolff and Ramos, 2013) up to ~1,125,000 km^3 estimated from seismic refraction profiles (Coffin and Eldholm, 1994), giving a total CRB magma volume of between 420,000 and 1,335,000 km^3. Intrusive magma degassing is more difficult to estimate than extrusive degassing though, and as a result this introduces additional uncertainty to our estimates of total magma degassing (Yoshimura and Nakamura, 2012). We define the ratio of the total emissions to just the extrusive emissions as the Emissions Amplification Factor (EAF), which based on our estimates is 2.0-6.4 for both our low and high degassing emission scenarios (Table 2). The emissions used in our simulations for each CRB formation are calculated by scaling the emission estimates for the whole CRB by the relative extrusive volume of these formations.

CRB magma may have also been further enriched in CO_2, H_2O, and other volatiles beyond the levels we assume in our calculations above due to crustal contamination of the magma feeding the eruptions, a process which Sobolev et al (2011) suggests caused significant additional degassing from the Siberian Traps. Both petrological studies and simulations of the origins of the CRB indicate that the magma feeding the CRB is likely to

have experienced similar crustal contamination and potential volatile enrichment prior to the GRB eruptions (Camp and Hanan, 2008; Liu and Stegman, 2012; Ramos et al., 2013; Rodriguez and Sen, 2013; Wolff and Ramos, 2013; Wolff et al., 2008), indicating that a similar amplification of emissions as hypothesised for the Siberian Traps may have occurred during the CRB eruptions. We crudely approximate the impact of these potential additional emissions simply by scaling the crust-contaminated emissions of the Siberian Traps hypothesised by Sobolev et al (2011) (~46,360 Pg C) by the volume of each CRB degassing source relative to the volume of the Siberian Traps (the total CRB being ~12 % the volume of the Siberian Traps) (Table 2). An EAF of 2.0-6.4 also applies to this crustal-contamination emission scenario.

An additional source of cryptic degassing beyond magma degassing is the metamorphism of the country rock, which is hypothesised to have caused large-scale emissions during other LIPs (e.g. Svensen et al., 2004). The scale of country rock metamorphosis associated with the CRB is partly obscured by the complex geology of the Columbia Basin, but the presence of carbonates, natural gas and coal in parts of the basin all point to a potentially significant source of additional carbon (LaMaskin et al., 2011; Lasmanis, 1991). Significant country rock degassing has been simulated to result from the intrusion of sills through various different lithologies, with a ~15 m thick sill intruding through organic-rich shale predicted to release ~1700 kg CH_4 per m^2 of sill extent (Aarnes et al., 2011a, 2011b). These simulations also suggest that metamorphic degassing of limestone and shale primarily releases CH_4 rather than CO_2 and so could further amplify the CRB's short-term warming potential, while the presence of evaporites could also lead to the release of ozone layer-damaging methyl chloride. If we assume that the Chief Joseph and Monument fissure-dykes that the GRB erupted from were fed by an underlying sill as part of a shallow dyke-sill complex (covering an area of ~100,000 km^2 for the Chief Joseph swarm; Fig. 2,

panel a; Reidel et al., 2013a; Rodriguez and Sen, 2013; Wolff and Ramos, 2013; Wolff et al., 2008), then this sill would yield metamorphic degassing emissions of up to ~1100 Pg C if the sill was intruded through coal, ~280 Pg C through limestones and ~2400 Pg C through organic-rich shale, while further metamorphic degassing would be expected from country rock dissected by the fissure dykes linked to this sill (Aarnes et al., 2011a). However, the extent of sills underlying the CRB and the total number, length and depth of the dykes of the Chief Joseph, Monument and other smaller dyke swarms remain poorly constrained, making it difficult to accurately estimate metamorphic degassing for the CRB. As a result we cautiously estimate that metamorphic degassing could yield on the order of an additional ~10^2-10^3 Pg of carbon, which would further amplify the maximum CRB cryptic degassing beyond our estimates in Table 2.

4. Results and Discussion

4.1. Modelled emission scenario

In Figure 4 we compare palaeorecords with model simulations for $\delta^{13}C$, CCD and atmospheric CO_2. We find that sub-aerial basalt degassing alone has a negligible effect in our simulations, but that adding cryptic degassing results in excursions similar to those seen in the palaeorecords. In some respects these results are counter-intuitive because they simulate: 1) a deepening of the CCD despite increasing atmospheric CO_2 and 2) a positive benthic $\delta^{13}C$ excursion despite the release of isotopically light (-4 ‰) volcanic carbon. The CCD result is attributable to the emission of carbon over a long (>10 ky) time-scale acting to stimulate increased terrestrial carbonate weathering such that the increased weathering flux of CO_3^{2-} to the ocean overcompensates for the initial reduction in [CO_3^{2-}] driven by ocean acidification (Fig. 5). The increase in benthic $\delta^{13}C$ is driven primarily by the $\delta^{13}C$ value of particulate

organic carbon (POC) becoming significantly lighter in response to increasing CO_2 as a result of the photosynthetic isotope effect, and partially by the increase in organic carbon burial due to increased productivity with increased riverine phosphorus delivery (Fig. 6) (Kump and Arthur, 1999). The burial of this light POC counteracts the further impact of the isotopically light volcanic carbon and leaves dissolved inorganic carbon and thus benthic foraminifera enriched in ^{13}C. Crust-contaminated magma, however, is predicted to emit CO_2 with an isotopic value of -12 ‰ (Sobolev et al. 2011) while country rock emissions can vary from 0 to 1.5 ‰ (from carbonates) to -20 to -50 ‰ (from shales, Table S3; Ganino and Arndt, 2009; Svensen et al., 2004). Our sensitivity analysis of volcanic $\delta^{13}C$ illustrates that giving volcanic carbon an isotopic value of -12 ‰ results in a $\delta^{13}C$ excursion similar to but slightly larger than in our best-fit simulation in MTW08 (Fig. S1), indicating that our main conclusions are not particularly sensitive to uncertainty in this parameter.

We find that in MTW08 an emission scenario of 1000 Pg C from the Steens and Imnaha eruptions, 3500 Pg C from the GRB eruptions and 280 Pg C from the Wanapum eruptions fit the palaeorecords prior to 15.4 Ma best, while in LOSCAR the best fit is found with slightly reduced emissions of 850 Pg C from the Steens and Imnaha eruptions, 3000 Pg from the GRB eruptions and 240 Pg from the Wanapum eruptions. The difference between the LOSCAR and MTW08 emission scenarios is primarily the result of the additional basalt weathering applied in MTW08, which implies that ~790 Pg C is drawn down by the weathering of fresh basalt during the CRB eruptions. Taking weathering uncertainties into account we estimate that a total CRB emission of 4090-5670 Pg C (an EAF of 6.3-8.7 based on the high degassing scenario or 4.2-5.8 based on the crust-contaminated scenario), with 3000-4000 Pg C of this emitted during just the GRB eruptions, best fits the palaeorecords. This emission range falls within the upper end of the range 460-6190 Pg C that we calculate to be feasible for the CRB (Table 2), demonstrating that a major perturbation to the long-term

carbon cycle and climate can only be achieved by invoking high degassing rates and a major contribution from cryptic degassing. Sensitivity analysis of the impact of the strength of the climate-weathering feedback indicates that although our results are moderately sensitive to the strength of this feedback (Fig. S2) it has to be significantly different from the values used in MTW08, LOSCAR and other models to significantly affect our results (Merico et al., 2008; Walker and Kasting, 1992; Walker et al., 1981; Zeebe, 2012). Sensitivity analysis of the impact of our choice of model parameters also indicates that our results are also moderately sensitive to the silicate weathering rate and sediment burial fraction of carbon export parameters in MTW08 (Fig. S3), but this sensitivity has a negligible impact on the overall result of requiring CRB carbon emissions greater than that possible from just sub-aerial basalt degassing in order to match the palaeorecords.

4.2. The CCD and the mid-Miocene Climate Transition

Both models fail to create the sustained CCD deepening seen in the palaeorecords, suggesting that some other mechanism drove part or all of the CCD deepening after ~15.4 Ma. A sustained CCD deepening can successfully be simulated through a combination of a shift in carbonate burial to the deep ocean and increased carbonate weathering as a result of ice-sheet growth causing sea-level to fall and shelf carbonate deposits to be exposed after 15.4 Ma or due to elevated continental weathering (simulated as a 30 % shelf burial reduction and a 20 % increase in carbonate weathering) (Barry et al., 2013; Kender et al., 2014; Merico et al., 2008; Passchier et al., 2011; Sandroni and Talarico, 2011; Shevenell et al., 2008) (Fig. 4). This result implies that the early Miocene CCD shoaling observed in the equatorial Pacific could be the result of reduced carbonate weathering rates and elevated sea levels associated with the mid-Miocene glacial minima which began at ~17.6 Ma (Passchier et al., 2011). Alternatively, the 16.0 Ma deepening could be the result of an increase in carbonate

productivity after a "carbonate famine" starting at 18.0 Ma (Lyle, 2003; Pälike et al., 2012), but no process able to drive this 2 My reduction of carbonate export has yet been proposed. A decrease in the $CaCO_3$:C_{org} rain ratio would also result in a CCD deepening via an increase in deep ocean [CO_3^{2-}], but this would also lead to an increase in benthic $\delta^{13}C$ in contradiction to the observed recovery in benthic $\delta^{13}C$ (Kender et al., 2014). As a result it is clear that, in our simulations, the permanent CCD deepening can be driven by the cooling trend resulting in shelf-basin carbonate fractionation and elevated carbonate weathering after ~15.4 Ma, but as the initial CCD deepening at ~16.0 Ma occurs during a time of relative warmth this suggests that the CRB had a role in deepening the CCD earlier than otherwise would have occurred (Feakins et al., 2012; Passchier et al., 2011). On the other hand it is important to note that the high-quality CCD records available from the eastern equatorial Pacific may not be globally representative, and that as the CCD shoalings at ~18.0 Ma and ~10.0 Ma (see Fig. 1) are unconnected to the CRB it is also possible that the ~16.0 Ma deepening may primarily be driven by a different process not discussed above. For other LIPs it is therefore likely that they could have also triggered a deepening of the CCD, but these deepenings may have been relatively transient and so may be difficult to observe in the low-resolution CCD palaeorecords currently available.

4.3. Mid-Miocene climate change

Proxy records and climate model simulations suggest that the warmth of the MCO (2 to 4 ^{o}C warmer than today) can be largely explained by atmospheric CO_2 concentrations increasing to >400 ppmv (Flower, 1999; Foster et al., 2012; Henrot et al., 2010; Herold et al., 2011; Knorr et al., 2011; Kürschner et al., 2008; You, 2010; You et al., 2009). Our simulations show a ~90 ppmv increase by 15.9 Ma, suggesting that at least some of this increase could have been derived from the CRB. This CO_2 increase would have increased

radiative forcing by 1.5 Wm^{-2} by 15.9 Ma (based on a CO_2 baseline of 280 ppmv), causing a global warming of 0.9 to 1.9 ^oC (assuming a climate sensitivity of 2.2 to 4.8 ^oC per CO_2 doubling; Rohling et al., 2012) compared to the observed mid-Miocene warmth of 2 to 4 ^oC relative to the Holocene. More warming could be achieved either with a higher climate sensitivity including slow feedbacks, with a long-term icehouse climate sensitivity of 6 ^oC per CO_2 doubling yielding 2.4 ^oC of warming (Hansen et al., 2008; Park and Royer, 2011), or from changes in other boundary conditions such as palaeogeography (Henrot et al., 2010; Herold et al., 2011; You et al., 2009). Although our estimate of CRB-driven temperature increase only reaches the lower limit of total mid-Miocene warming it does coincide with the second MCO warmth maximum and ice sheet extent minimum around 15.7 Ma, implying that the CRB could have helped intensify the MCO and delayed the subsequent reglaciation of the Antarctic during the mid-Miocene Climate Transition (Billups and Schrag, 2003; Feakins et al., 2012; Foster et al., 2012; Holbourn et al., 2013, 2007; Passchier et al., 2011; Shevenell et al., 2008). However, the first MCO warmth maximum at ~16.5 Ma pre-dates the simulated onset of the GRB cryptic degassing by ~200 ky and is preceded by the relatively small emissions of the Steens and Imnaha basalt eruptions, implying that the CRB was not the sole cause of the MCO. The timing of the equatorial Pacific CCD deepening also suggests there was no major pulse in emissions before ~16.3 Ma as no major changes in the CCD are observed between 18.0 and 16.0 Ma. These observations imply that some other process may have driven warming independently of the CRB in the early stages of the MCO, and that this process may also be linked to the ~18.0 Ma CCD shoaling and the MCIE. Other LIPs may have also occurred during similar times of background climate variability, thus complicating the interpretation of LIP-driven climate change and emphasizing the importance of establishing an accurate chronology of eruption phases and climate events when establishing the magnitude of LIP-driven climate change.

The timing of our best-fit emissions scenario also implies that the GRB cryptic degassing began around the same time as the 'Mi-2' glacial maximum at ~16.2 Ma (Miller et al., 1991). It is possible that enough sulphate aerosols and other volatiles may have been released to have triggered an initial, short-term episode of cooling prior to the longer-term warming effect of CO_2 becoming dominant (Sobolev et al., 2011; Thordarson and Self, 1996). The Deccan Traps and other LIPs are estimated to have released ~7 Tg SO_2 km^{-3}, which implies an emission of ~$1.1x10^3$ Pg SO_2 (an emission rate of ~2.6 Tg SO_2 y^{-1} over 400 ky) from the GRB sub-aerial basalts and up to ~$9.3x10^3$ Pg SO_2 (~23.4 Tg SO_2 y^{-1}) for the maximum total GRB volume (Self et al., 2006). This is significantly more than the background atmosphere SO_2 content of <1 Tg, implying that GRB cryptic degassing could have initially triggered global cooling before the gradual increase in atmospheric CO_2 led to warming dominating as cryptic degassing reached its end. It is well established that larger LIPs are associated with significant releases of SO_2 (Self et al., 2006; Sobolev et al., 2011; Wignall, 2001), but our results imply that other small LIPs may also coincide with an initial episode of cooling prior to longer-term warming peaking after eruptions decline.

5. Conclusions

We find that we can successfully simulate perturbations to the benthic $\delta^{13}C$, the CCD and atmospheric CO_2 palaeorecords at ~16.0 Ma with the emission of 4090-5670 Pg C from the CRB, of which 3000-4000 Pg C is emitted during the GRB eruptions between 16.3 and 15.9 Ma, and that the CRB is capable of these emissions if a major role is invoked for cryptic degassing from intrusive volcanic activity. Even this emission scenario cannot account for the warmth of the entire MCO though, implying that some other driver of global warmth existed prior to 16.3 Ma, and we also find that some other process after 15.4 Ma such as reglaciation must have occurred to keep the CCD deepened after this time. If the same cryptic degassing

sources were involved in other LIPs then our results imply that those LIPs would have also had a more significant impact on global climate and ocean biogeochemistry than previously estimated and their impacts therefore require reappraisal.

Acknowledgements

This work was supported by a Natural Environment Research Council studentship to D.I.A.M (grant number NE/J500112/1). We thank Agostino Merico and Richard Zeebe for sharing their respective models and advice on using them, Heiko Pälike and Ann Holbourn for sharing their data, Jon Blundy for comments on the likely extent of intrusive and underplated magma, and Kevin Oliver, Lee Kump, Ellen Thomas and several anonymous reviewers for constructive feedback on earlier drafts of this manuscript.

References

Aarnes, I., Fristad, K., Planke, S., Svensen, H., 2011a. The impact of host-rock composition on devolatilization of sedimentary rocks during contact metamorphism around mafic sheet intrusions. Geochemistry, Geophys. Geosystems 12.

Aarnes, I., Podladchikov, Y., Svensen, H., 2012. Devolatilization-induced pressure build-up: Implications for reaction front movement and breccia pipe formation. Geofluids 12, 265–279.

Aarnes, I., Svensen, H., Polteau, S., Planke, S., 2011b. Contact metamorphic devolatilization of shales in the Karoo Basin, South Africa, and the effects of multiple sill intrusions. Chem. Geol. 281, 181–194.

Baksi, A.K., 2013. Timing and duration of volcanism in the Columbia River Basalt Group: A review of existing radiometric data and new constraints on the age of the Steens through Wanapum Basalt extrusion. Geol. Soc. Am. Spec. Pap. 497, 67–85.

Barry, T.L., Kelley, S.P., Camp, V.E., Self, S., Jarboe, N.A., Duncan, R., 2013. Eruption chronology of the Columbia River Basalt Group, in: Reidel, S.P., Camp, V.E., Ross, M.E., Wolff, J.A., Martin, B.S., Tolan, T.L., Wells, R.. (Eds.), The Columbia River Flood Basalt Province: Geological Society of America Special Paper 497. pp. 45–66.

Barry, T.L., Self, S., Kelley, S.P., Reidel, S.P., Hooper, P.R., Widdowson, M., 2010. New 40Ar/39Ar dating of the Grande Ronde lavas, Columbia River Basalts, USA: Implications for duration of flood basalt eruption episodes. Lithos 118, 213–222.

Beerling, D.J., Royer, D.L., 2011. Convergent Cenozoic CO2 history. Nat. Geosci. 4, 418–420.

Billups, K., Schrag, D.P., 2003. Application of benthic foraminiferal Mg/Ca ratios to questions of Cenozoic climate change. Earth Planet. Sci. Lett. 209, 181–195.

Bryan, S.E., Ernst, R.E., 2008. Revised definition of Large Igneous Provinces (LIPs). Earth-Science Rev. 86, 175–202.

Caldeira, K., Rampino, M.R., 1990. Carbon dioxide emissions from Deccan Volcanism and a K/T boundary greenhouse effect. Geophys. Res. Lett. 17, 1299–1302.

Camp, V.E., Hanan, B.B., 2008. A plume-triggered delamination origin for the Columbia River Basalt Group. Geosphere 4, 480.

Coffin, M.F., Eldholm, O., 1994. Large Igneous Provinces: crustal structure, dimensions, and external consequences. Rev. Geophys. 32, 1–36.

Courtillot, V.E., Renne, P.R., 2003. On the ages of flood basalt events. Comptes Rendus Geosci. 335, 113–140.

Dessert, C., Dupré, B., Gaillardet, J., François, L.M., Allègre, C.J., 2003. Basalt weathering laws and the impact of basalt weathering on the global carbon cycle. Chem. Geol. 202, 257–273.

Diester-Haass, L., Billups, K., Gröcke, D.R., François, L.M., Lefebvre, V., Emeis, K.C., 2009. Mid-Miocene paleoproductivity in the Atlantic Ocean and implications for the global carbon cycle. Paleoceanography 24, 1–19.

Ernst, R.E., Buchan, K.L., Campbell, I.H., 2005. Frontiers in large igneous province research. Lithos 79, 271–297.

Erwin, D.H., 2006. Extinction: how life on Earth nearly ended 250 million years ago. Princeton University Press, Princeton.

Feakins, S.J., Warny, S., Lee, J.-E., 2012. Hydrologic cycling over Antarctica during the middle Miocene warming. Nat. Geosci. 5, 557–560.

Flower, B.P., 1999. Cenozoic Deep-Sea Temperatures and Polar Glaciation : the Oxygen Isotope Record. Terra Antart. Reports 3, 27–42.

Foster, G.L., Lear, C.H., Rae, J.W.B., 2012. The evolution of pCO2, ice volume and climate during the middle Miocene. Earth Planet. Sci. Lett. 341-344, 243–254.

Ganino, C., Arndt, N.T., 2009. Climate changes caused by degassing of sediments during the emplacement of large igneous provinces. Geology 37, 323–326.

Ganino, C., Arndt, N.T., 2010. Climate changes caused by degassing of sediments during the emplacement of large igneous provinces: REPLY. Geology 38, e211.

Grard, A., Francois, L., Dessert, C., Dupré, B., Goddéris, Y., 2005. Basaltic volcanism and mass extinction at the Permo-Triassic boundary: Environmental impact and modeling of the global carbon cycle. Earth Planet. Sci. Lett. 234, 207–221.

Haefner, J.W., 1996. Modeling Biological Systems: Principles and Applications. Chapman and Hull.

Hansen, J., Sato, M., Kharecha, P., Beerling, D.J., Berner, R.A., Masson-delmotte, V., Pagani, M., Raymo, M., Royer, D.L., Zachos, J.C., 2008. Target Atmospheric CO2 : Where Should Humanity Aim? Open Atmos. Sci. J. 217–231.

Hartmann, J., Moosdorf, N., 2011. Chemical weathering rates of silicate-dominated lithological classes and associated liberation rates of phosphorus on the Japanese Archipelago—Implications for global scale analysis. Chem. Geol. 287, 125–157.

Henrot, A.-J., François, L.M., Favre, E., Butzin, M., Ouberdous, M., Munhoven, G., 2010. Effects of CO2, continental distribution, topography and vegetation changes on the climate at the Middle Miocene: a model study. Clim. Past 6, 675–694.

Herold, N., Huber, M., Müller, R.D., 2011. Modeling the Miocene Climatic Optimum. Part I: Land and Atmosphere*. J. Clim. 24, 6353–6372.

Hodell, D.A., Woodruff, F., 1994. Variations in the strontium isotopic ratio of seawater during the Miocene: Stratigraphic and geochemical implications. Paleoceanography 9, 405–426.

Holbourn, A., Kuhnt, W., Lyle, M.W., Schneider, L.J., Romero, O., Andersen, N., 2013. Middle Miocene climate cooling linked to intensification of eastern equatorial Pacific upwelling. Geology 42, 19–22.

Holbourn, A., Kuhnt, W., Schulz, M., Flores, J.-A., Andersen, N., 2007. Orbitally-paced climate evolution during the middle Miocene "Monterey" carbon-isotope excursion. Earth Planet. Sci. Lett. 261, 534–550.

Hooper, P.R., 1988. The Columbia River Basalt, in: Macdougall, J.D. (Ed.), Continental Flood Basalts. Kluwer Academic Publishers, Dordrecht, The Netherlands, pp. 1–33.

Hooper, P.R., 1997. The Columbia River Flood Basalt: Current Status, in: Mahoney, J.J., Coffin, M.F. (Eds.), Large Igneous Provinces: Continental, Oceanic, and Planetary Flood Volcanism. American Geophysical Union, Washington DC, pp. 1–27.

Iacono-Marziano, G., Marecal, V., Pirre, M., Gaillard, F., Arteta, J., Scaillet, B., Arndt, N.T., 2012. Gas emissions due to magma–sediment interactions during flood magmatism at

the Siberian Traps: Gas dispersion and environmental consequences. Earth Planet. Sci. Lett. 357-358, 308–318.

Jarboe, N.A., Coe, R.S., Renne, P.R., Glen, J.M.G., 2010. The age of the Steens reversal and the Columbia River Basalt Group. Chem. Geol. 274, 158–168.

Karlstrom, L., Richards, M., 2011. On the evolution of large ultramafic magma chambers and timescales for flood basalt eruptions. J. Geophys. Res. 116, 1–13.

Kender, S., Peck, V.L., Jones, R.W., Kaminski, M.A., 2009. Middle Miocene oxygen minimum zone expansion offshore West Africa: Evidence for global cooling precursor events. Geology 37, 699–702.

Kender, S., Yu, J., Peck, V.L., 2014. Deep ocean carbonate ion increase during mid Miocene CO2 decline. Sci. Rep. 4, 1–6.

Knorr, G., Butzin, M., Micheels, A., Lohmann, G., 2011. A warm Miocene climate at low atmospheric CO2 levels. Geophys. Res. Lett. 38, 1–5.

Kump, L.R., Arthur, M.A., 1999. Interpreting carbon-isotope excursions: carbonates and organic matter. Chem. Geol. 161, 181–198.

Kürschner, W.M., Kvacek, Z., Dilcher, D.L., 2008. The impact of Miocene atmospheric carbon dioxide fluctuations on climate and the evolution of terrestrial ecosystems. Proc. Natl. Acad. Sci. U. S. A. 105, 449–53.

LaMaskin, T.A., Vervoort, J.D., Dorsey, R.J., Wright, J.E., 2011. Early Mesozoic paleogeography and tectonic evolution of the western United States: Insights from detrital zircon U-Pb geochronology, Blue Mountains Province, northeastern Oregon. Geol. Soc. Am. Bull. 123, 1939–1965.

Lasmanis, R., 1991. The geology of Washington. Rocks Miner. 66, 262–277.

Liu, L., Stegman, D.R., 2012. Origin of Columbia River flood basalt controlled by propagating rupture of the Farallon slab. Nature 482, 386–9.

Lyle, M.W., 2003. Neogene carbonate burial in the Pacific Ocean. Paleoceanography 18, 1–19.

Lyle, M.W., Pälike, H., Nishi, H., Raffi, I., Gamage, K., Klaus, A., 2010. The Pacific Equatorial Age Transect, IODP Expeditions 320 and 321: Building a 50-Million-Year-Long Environmental Record of the Equatorial Pacific Ocean. Sci. Drill.

Menand, T., Phillips, J.C., 2007. Gas segregation in dykes and sills. J. Volcanol. Geotherm. Res. 159, 393–408.

Merico, A., Tyrrell, T., Wilson, P.A., 2008. Eocene/Oligocene ocean de-acidification linked to Antarctic glaciation by sea-level fall. Nature 452, 979–82.

Miller, K.G., Wright, J.D., Fairbanks, G., 1991. Unlocking the Ice House: Oligocene-Miocene Oxygen Isotopes, Eustasy, and Margin Erosion. J. Geophys. Res. 96, 6829–6848.

Pälike, H., Lyle, M.W., Nishi, H., Raffi, I., Ridgwell, A.J., Gamage, K., Klaus, A., Acton, G., Anderson, L., Backman, J., Baldauf, J., Beltran, C., Bohaty, S.M., Bown, P.R., Busch, W., Channell, J.E.T., Chun, C.O.J., Delaney, M.L., Dewangan, P., Dunkley Jones, T., Edgar, K.M., Evans, H., Fitch, P., Foster, G.L., Gussone, N., Hasegawa, H., Hathorne, E.C., Hayashi, H., Herrle, J.O., Holbourn, A., Hovan, S., Hyeong, K., Iijima, K., Ito, T., Kamikuri, S., Kimoto, K., Kuroda, J., Leon-Rodriguez, L., Malinverno, A., Moore Jr., T.C., Murphy, B.H., Murphy, D.P., Nakamura, H., Ogane, K., Ohneiser, C., Richter, C.,

519 Robinson, R., Rohling, E.J., Romero, O., Sawada, K., Scher, H., Schneider, L., Sluijs,
520 A., Takata, H., Tian, J., Tsujimoto, A., Wade, B.S., Westerhold, T., Wilkens, R.,
521 Williams, T., Wilson, P.A., Yamamoto, Y., Yamamoto, S., Yamazaki, T., Zeebe, R.E.,
522 2012. A Cenozoic record of the equatorial Pacific carbonate compensation depth. Nature
523 488, 609–614.

524 Park, J., Royer, D.L., 2011. Geologic constraints on the glacial amplification of Phanerozoic
525 climate sensitivity. Am. J. Sci. 311, 1–26.

526 Passchier, S., Browne, G., Field, B., Fielding, C.R., Krissek, L.A., Panter, K., Pekar, S.F.,
527 2011. Early and middle Miocene Antarctic glacial history from the sedimentary facies
528 distribution in the AND-2A drill hole, Ross Sea, Antarctica. Geol. Soc. Am. Bull. 123,
529 2352–2365.

530 Ramos, F.C., Wolff, J.A., Starkel, W., Eckberg, A., Tollstrup, D.L., Scott, S., 2013. The
531 changing nature of sources associated with Columbia River fl ood basalts: Evidence
532 from strontium isotope ratio variations in plagioclase phenocrysts. Geol. Soc. Am. Spec.
533 Pap. 497, 231–257.

534 Reidel, S.P., Camp, V.E., Tolan, T.L., Kauffman, J.D., Garwood, D.L., 2013a. Tectonic
535 evolution of the Columbia River flood basalt province. Geol. Soc. Am. Spec. Pap. 497,
536 293–324.

537 Reidel, S.P., Camp, V.E., Tolan, T.L., Martin, B.S., 2013b. The Columbia River flood basalt
538 province: Stratigraphy, areal extent, volume, and physical volcanology. Geol. Soc. Am.
539 Spec. Pap. 497, 1–43.

540 Reidel, S.P., Tolan, T.L., 2013. The Grande Ronde Basalt, Columbia River Basalt Group.
541 Geol. Soc. Am. Spec. Pap. 497, 117–153.

542 Retallack, G.J., Jahren, A.H., 2008. Methane Release from Igneous Intrusion of Coal during
543 Late Permian Extinction Events. J. Geol. 116, 1–20.

544 Rodriguez, S., Sen, G., 2013. Eruption of the Grande Ronde Basalt lavas, Columbia River
545 Basalt Group: Results of numerical modeling. Geol. Soc. Am. Spec. Pap. 497, 259–272.

546 Rohling, E.J., Sluijs, A., Dijkstra, H.A., Köhler, P., van de Wal, R.S.W., von der Heydt, A.S.,
547 Beerling, D.J., Berger, A., Bijl, P.K., Crucifix, M., DeConto, R.M., Drijfhout, S.S.,
548 Fedorov, A., Foster, G.L., Ganopolski, A., Hansen, J., Hönisch, B., Hooghiemstra, H.,
549 Huber, M., Huybers, P., Knutti, R., Lea, D.W., Lourens, L.J., Lunt, D.J., Masson-
550 Demotte, V., Medina-Elizalde, M., Otto-Bliesner, B., Pagani, M., Pälike, H., Renssen,
551 H., Royer, D.L., Siddall, M., Valdes, P.J., Zachos, J.C., Zeebe, R.E., 2012. Making
552 sense of palaeoclimate sensitivity. Nature 491, 683–91.

553 Sandroni, S., Talarico, F.M., 2011. The record of Miocene climatic events in AND-2A drill
554 core (Antarctica): Insights from provenance analyses of basement clasts. Glob. Planet.
555 Change 75, 31–46.

556 Self, S., Widdowson, M., Thordarson, T., Jay, A.E., 2006. Volatile fluxes during flood basalt
557 eruptions and potential effects on the global environment: A Deccan perspective. Earth
558 Planet. Sci. Lett. 248, 518–532.

559 Shevenell, A.E., Kennett, J.P., Lea, D.W., 2008. Middle Miocene ice sheet dynamics, deep-
560 sea temperatures, and carbon cycling: A Southern Ocean perspective. Geochemistry
561 Geophys. Geosystems 9.

562 Shinohara, H., 2008. Excess degassing from volcanoes and its role on eruptive and intrusive
563 activity. Rev. Geophys. 46, 1–31.

564 Sobolev, S. V., Sobolev, A. V., Kuzmin, D. V., Krivolutskaya, N.A., Petrunin, A.G., Arndt,
565 N.T., Radko, V.A., Vasiliev, Y.R., 2011. Linking mantle plumes, large igneous
566 provinces and environmental catastrophes. Nature 477, 312–316.

567 Svensen, H., Planke, S., Malthe-Sørenssen, A., Jamtveit, B., Myklebust, R., Rasmussen
568 Eidem, T., Rey, S.S., 2004. Release of methane from a volcanic basin as a mechanism
569 for initial Eocene global warming. Nature 429, 542–545.

570 Svensen, H., Planke, S., Polozov, A.G., Schmidbauer, N., Corfu, F., Podladchikov, Y.Y.,
571 Jamtveit, B., 2009. Siberian gas venting and the end-Permian environmental crisis. Earth
572 Planet. Sci. Lett. 277, 490–500.

573 Taylor, A.S., Lasaga, A.C., 1999. The role of basalt weathering in the Sr isotope budget of
574 the oceans. Chem. Geol. 161, 199–214.

575 Thordarson, T., Self, S., 1996. Sulfur, chlorine and fluorine degassing and atmospheric
576 loading by the Roza eruption, Columbia River Basalt Group, Washington, USA. J.
577 Volcanol. Geotherm. Res. 74, 49–73.

578 Vincent, E., Berger, W.H., 1985. Carbon dioxide and polar cooling in the Miocene: The
579 Monterey hypothesis, in: Broecker, W.S., Sundquist, E.T. (Eds.), The Carbon Cycle and
580 Atmospheric CO2: Natural Variations Archean to Present, Geophys. Monogr. Ser., Vol.
581 32. AGU, Washington, D. C., pp. 455–468.

582 Walker, J.C.G., Hays, P.B., Kasting, J.F., 1981. A negative feedback mechanism for the long-
583 term stabilization of Earth's surface temperature. J. Geophys. Res. 86, 9776–9782.

584 Walker, J.C.G., Kasting, J.F., 1992. Effects of fuel and forest conservation on future levels of
585 atmospheric carbon dioxide. Palaeogeogr. Palaeoclimatol. Palaeoecol. 97, 151–89.

586 Wignall, P., 2001. Large igneous provinces and mass extinctions. Earth-Science Rev. 53, 1–
587 33.

588 Wignall, P., 2005. The Link between Large Igneous Province Eruptions and Mass
589 Extinctions. Elements 1, 293–297.

590 Wolff, J.A., Ramos, F.C., 2013. Source materials for the main phase of the Columbia River
591 Basalt Group: Geochemical evidence and implications for magma storage and transport.
592 Geol. Soc. Am. Spec. Pap. 497, 273–291.

593 Wolff, J.A., Ramos, F.C., Hart, G.L., Patterson, J.D., Brandon, A.D., 2008. Columbia River
594 flood basalts from a centralized crustal magmatic system. Nat. Geosci. 1, 177–180.

595 Yoshimura, S., Nakamura, M., 2012. Flux of volcanic CO2 emission estimated from melt
596 inclusions and fluid transport modelling. Earth Planet. Sci. Lett. 361, 497–503.

597 You, Y., 2010. Climate-model evaluation of the contribution of sea-surface temperature and
598 carbon dioxide to the Middle Miocene Climate Optimum as a possible analogue of
599 future climate change. Aust. J. Earth Sci. 57, 207–219.

600 You, Y., Huber, M., Müller, R.D., Poulsen, C.J., Ribbe, J., 2009. Simulation of the Middle
601 Miocene Climate Optimum. Geophys. Res. Lett. 36, 1–5.

602 Zachos, J.C., Dickens, G.R., Zeebe, R.E., 2008. An early Cenozoic perspective on
603 greenhouse warming and carbon-cycle dynamics. Nature 451, 279–83.

604 Zeebe, R.E., 2012. LOSCAR: Long-term Ocean-atmosphere-Sediment CArbon cycle
605 Reservoir Model v2.0.4. Geosci. Model Dev. 5, 149–166.

606 Zeebe, R.E., Zachos, J.C., Dickens, G.R., 2009. Carbon dioxide forcing alone insufficient to
607 explain Palaeocene–Eocene Thermal Maximum warming. Nat. Geosci. 2, 576–580.

608 Zhang, Y.G., Pagani, M., Liu, Z., Bohaty, S.M., DeConto, R.M., 2013. A 40-million-year
609 history of atmospheric CO2. Philos. Trans. R. Soc. London. Ser. A 371.

610 **Figures (Web Version)**

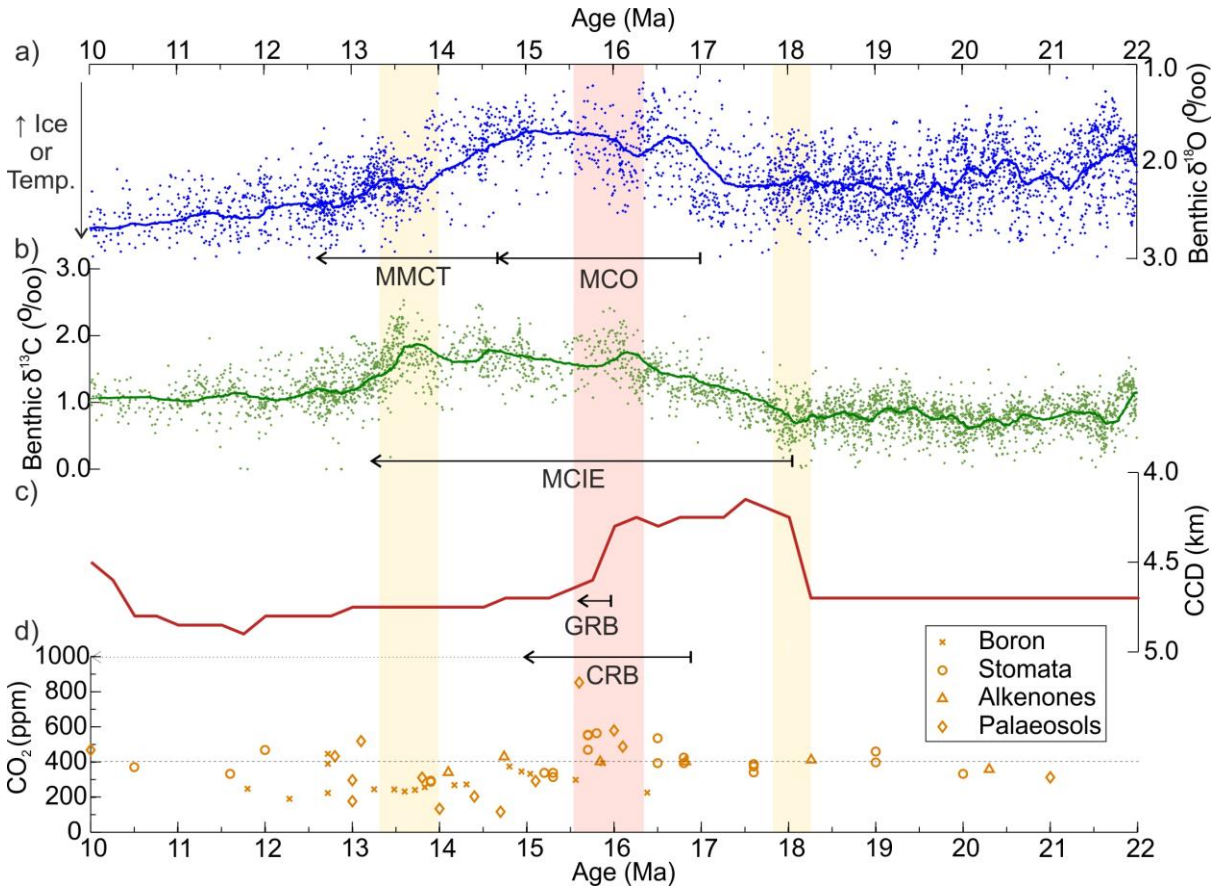

611

612 **Figure 1:** Comparison of palaeorecords between 10 and 22 Ma of: benthic foraminifera
613 a) $\delta^{13}C$ (black (green in the web version) dots) and b) $\delta^{18}O$(black (blue in the web version)
614 dots) compilations and their secular trends (solid black (blue/green in the web version) lines
615 illustrate the 100-point moving average) (Zachos et al., 2008), c) equatorial Pacific CCD
616 palaeodepth (solid black (red solid in the web version) line; Pälike et al., 2012), and d)
617 atmospheric CO_2 reconstructed using boron (black (orange in the web version) crosses;
618 Foster et al., 2012), alkenone (black (orange in the web version) triangles; Zhang et al.,
619 2013), stomata and palaeosol (black (orange in the web version) circles and diamonds,
620 respectively; Beerling and Royer, 2011) based techniques with the 400 ppm level marked by
621 the dashed black line. The durations of the Miocene Climatic Optimum (MCO), mid-Miocene
622 Climate Transition (MMCT), Monterey Carbon Isotope Excursion (MCIE), Columbia River
623 Basalt (CRB) main eruption phase (with the minor Saddle Mountain eruptions shown by

624 dotted arrow) and the Grande Ronde Basalt (GRB) eruptions are illustrated. Perturbations to
625 the palaeorecords at ~18.0, ~16.0 and ~14.0 Ma are highlighted by the grey (orange and red
626 in the web version) bars, with the dark grey (red in the web version) bar marking the
627 perturbation which is the focus of this study and shown in greater detail in Figure 3.

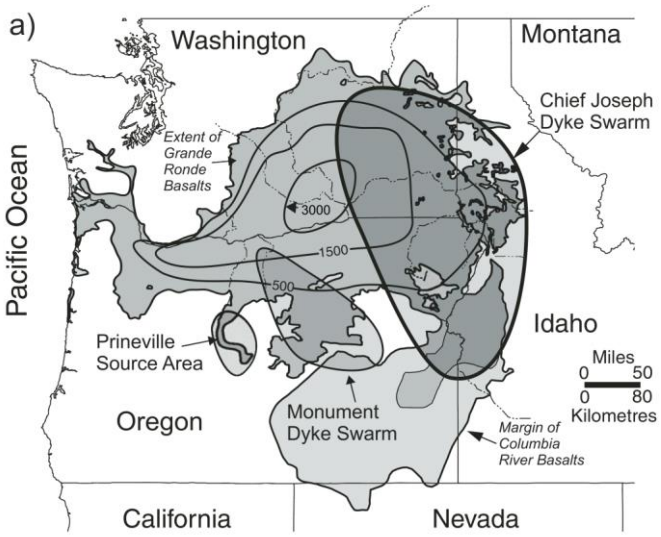

b)

CRB formation	Volume (km^3)	Age (Ma)
Wanapum Basalt	12,000	15.0
		15.6
Eruption interval		
Grande Ronde Basalt (GRB)	152,000	15.9
Imnaha Basalt	11,000	16.3
Steens Basalt	32,000	16.8

Figure 2: a) Map illustrating the location and the extent of the Columbia River Basalts (CRB), the Grande Ronde Basalt (GRB) formation within the CRB (with the GRB's thickness in metres illustrated by the isopachs) and the GRB's associated dyke swarms. Figure adapted from Reidel et al. (2013b). b) Illustration of the main Columbia River Basalt formations with each formation's extrusive volume (to the nearest 1000 km^3; Reidel et al., 2013b) and the CRB eruption chronology used in this study.

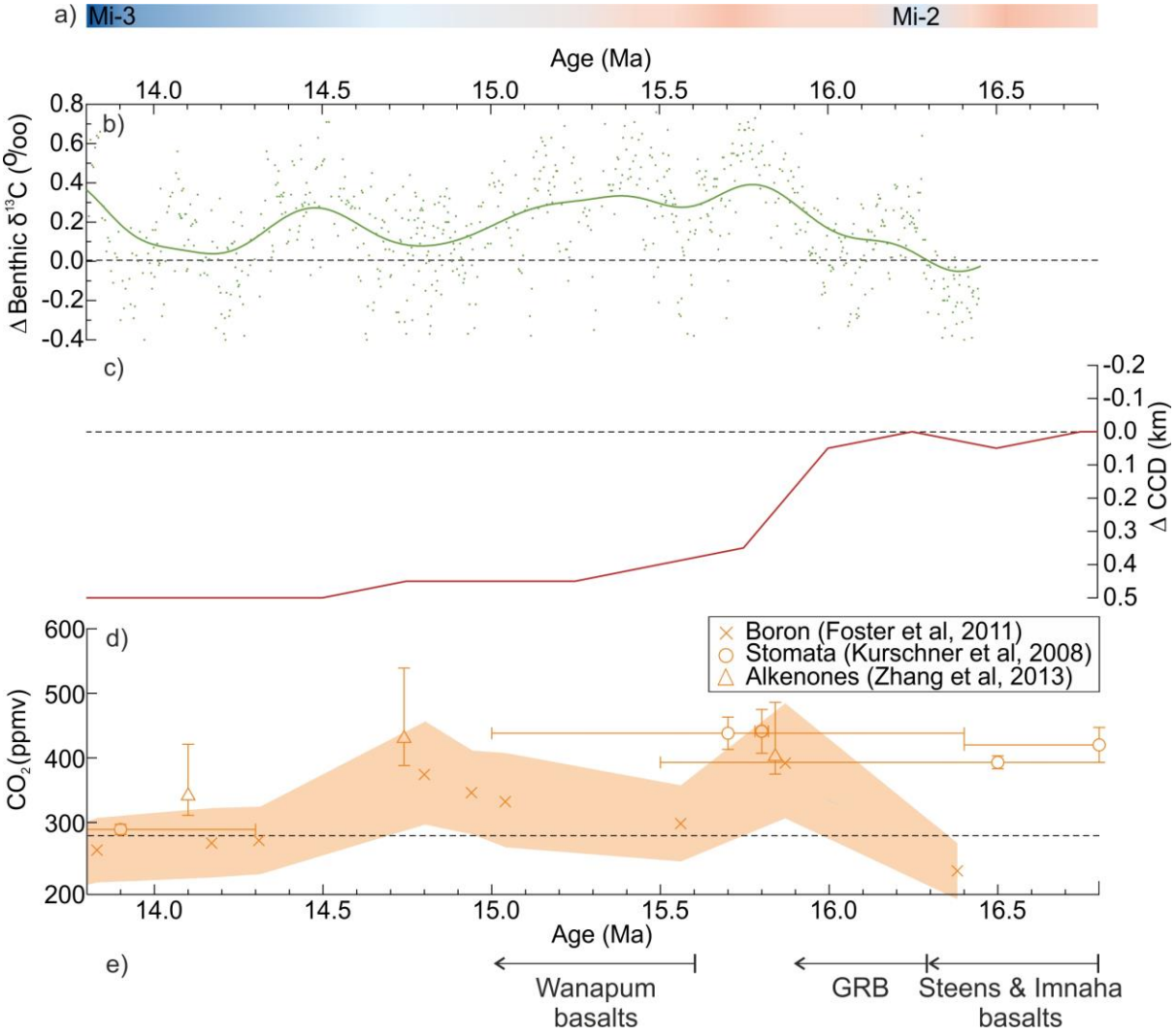

Figure 3: a) Occurrence of Antarctic glacial minima and maxima marked by the dark (red in the web version) and light (blue in the web version) bars respectively with 'Mi-2' and 'Mi-3' glaciations labelled (Feakins et al., 2012; Miller et al., 1991; Passchier et al., 2011). Palaeorecords of: b) benthic foraminifera $\delta^{13}C$ from IODP site 1146 (black (green in the web version) dots) and its secular trend (calculated by using a Gaussian filter to remove signals below 420 ky; solid black (green in the web version) line; Δ=0 pinned at 16.3 Ma) (Holbourn et al., 2007), c) reconstruction of CCD palaeodepth in the equatorial Pacific (solid black (red in the web version) line; Δ=0 pinned at 16.3 Ma; Pälike et al., 2012), and d) reconstructions of atmospheric CO_2 based on boron isotopes (black (orange in the web version) crosses with grey (orange in the web version) band for error; Foster et al., 2012), leaf stomata (black

(orange in the web version) circles with error bars; Kürschner et al., 2008) and alkenone $\delta^{13}C$ (black (orange in the web version) triangles with error bars; Zhang et al., 2013).

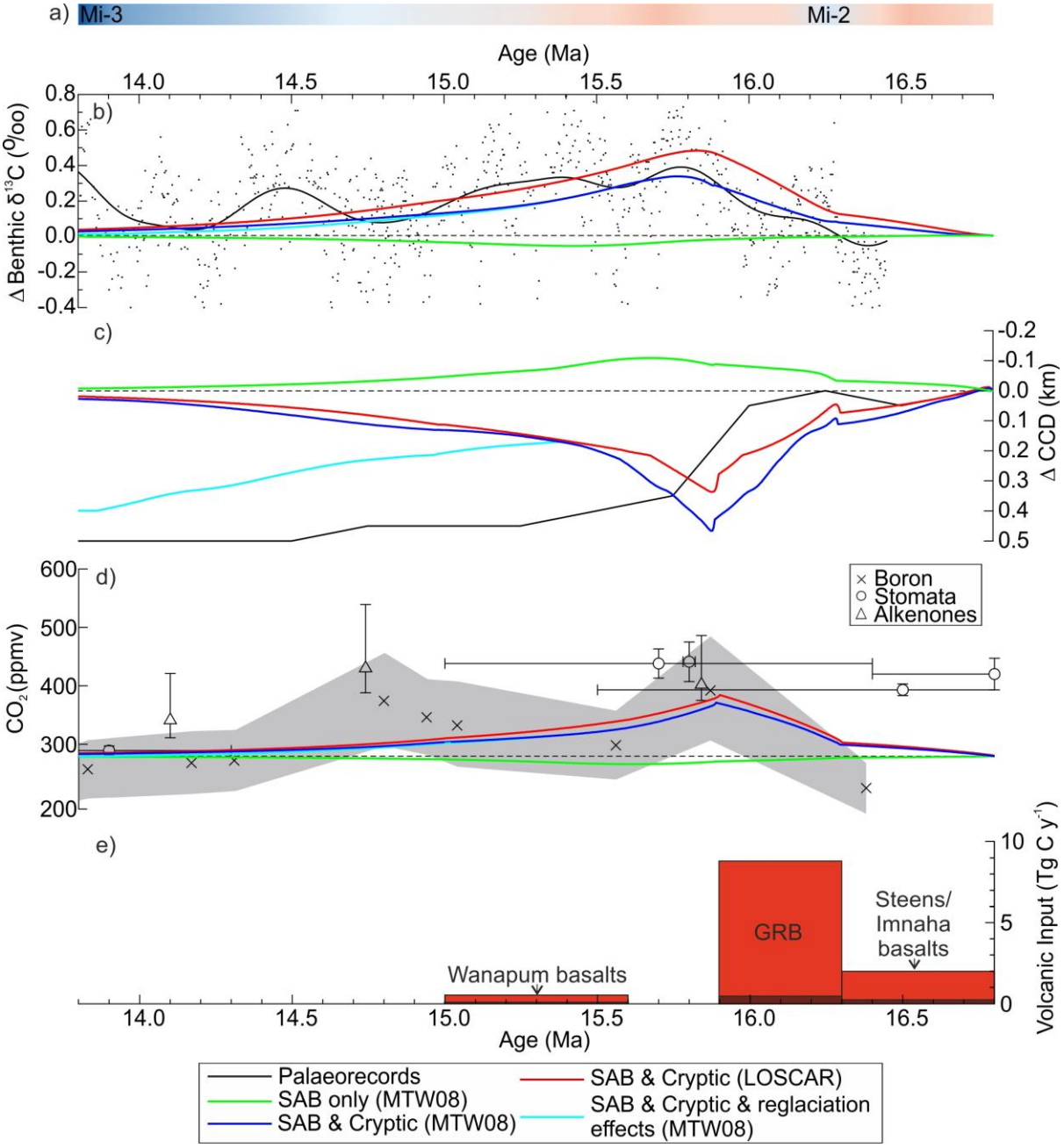

Figure 4: a) Occurrence of Antarctic glacial minima and maxima marked by the dark (red in the web version) and light (blue in the web version) bars respectively with the Mi-2 and Mi-3 glaciations labelled (Feakins et al., 2012; Miller et al., 1991; Passchier et al., 2011). Model results relative to steady-state values of: b) benthic $\delta^{13}C$ (benthic foraminifera in MTW08, deep ocean dissolved inorganic carbon in LOSCAR), c) CCD palaeodepth (global in MTW08, Pacific in LOSCAR) and d) atmospheric CO_2 for our sub-aerial basalt degassing only simulation in MTW08 (dot-dashed (green in the web version) line), our best-fit MTW08

simulation (solid black (solid dark blue in the web version) line, with additional run with post-CRB glaciation effects shown by the dashed black (solid light blue in the web version) line) and our best-fit LOSCAR simulation (dotted black (red in the web version) line); plotted against palaeorecords (each with Δ=0 pinned to either models' steady-state value at 16.3 Ma for the relevant model output, presented here in grey (black in the web version) for clarity instead of the colours shown in Figure 2) of: b) benthic foraminifera $\delta^{13}C$ from IODP site 1146 (dots) and its secular trend (solid line) (Holbourn et al., 2007), c) reconstruction of CCD palaeodepth in the equatorial Pacific (solid line) (Pälike et al., 2012), and d) reconstructions of atmospheric CO_2 based on boron isotopes (crosses, light grey band for error; Foster et al., 2012), leaf stomata (circles with error bars; Kürschner et al., 2008) and alkenone $\delta^{13}C$ (triangles with error bars; Zhang et al., 2013). e) Volcanic emissions scenario for the best-fit MTW08 scenario divided according to CRB formation and emission source (cryptic degassing, grey (red in the web version); sub-aerial basalt degassing, black (dark red in the web version)).

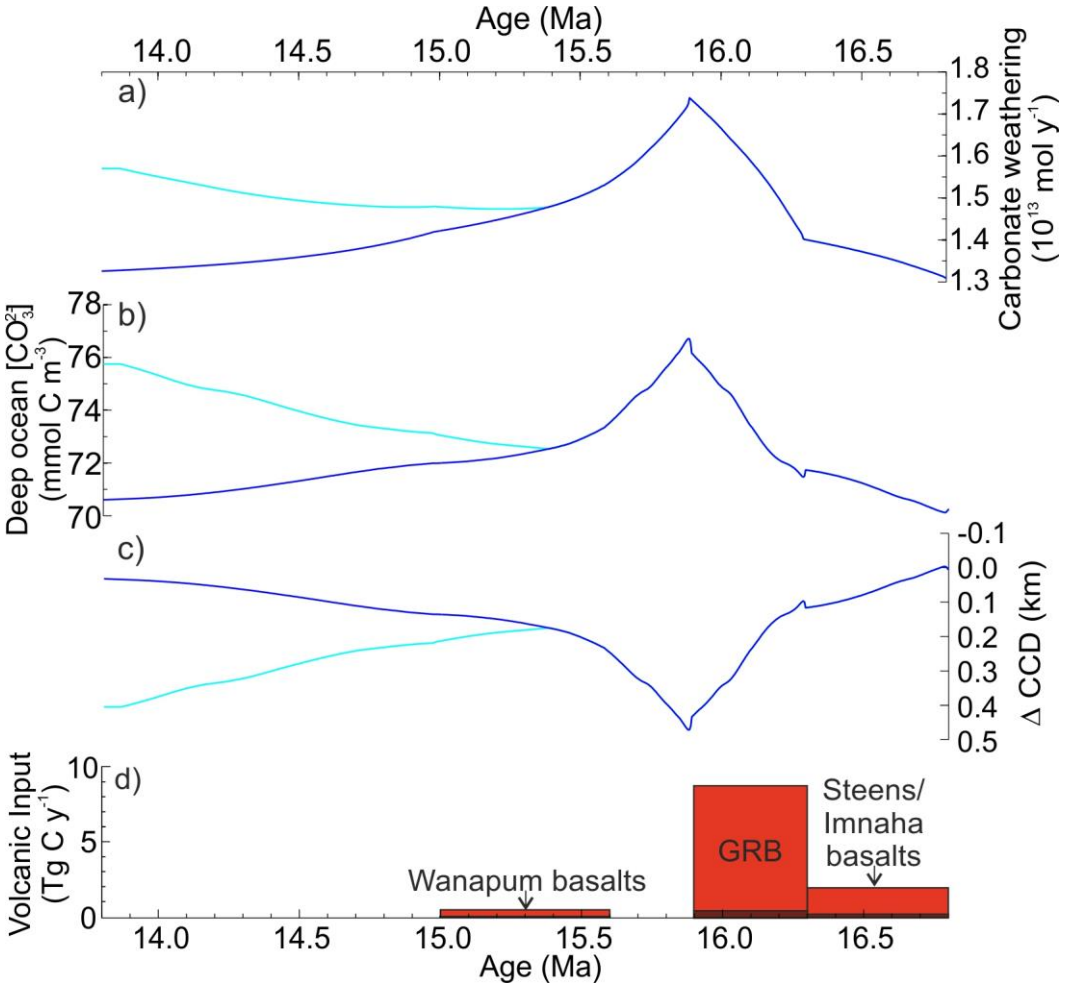

670

671 **Figure 5:** Simulation results in MTW08 of: a) carbonate weathering flux, b) deep ocean
672 carbonate ion concentration and c) change in CCD (relative to 16.3 Ma) for our best-fit
673 MTW08 emissions scenario illustrated in panel d) (solid black (dark blue in the web version)
674 line, with additional run with post-CRB glaciation effects shown by the dashed black (light
675 blue in the web version) line).

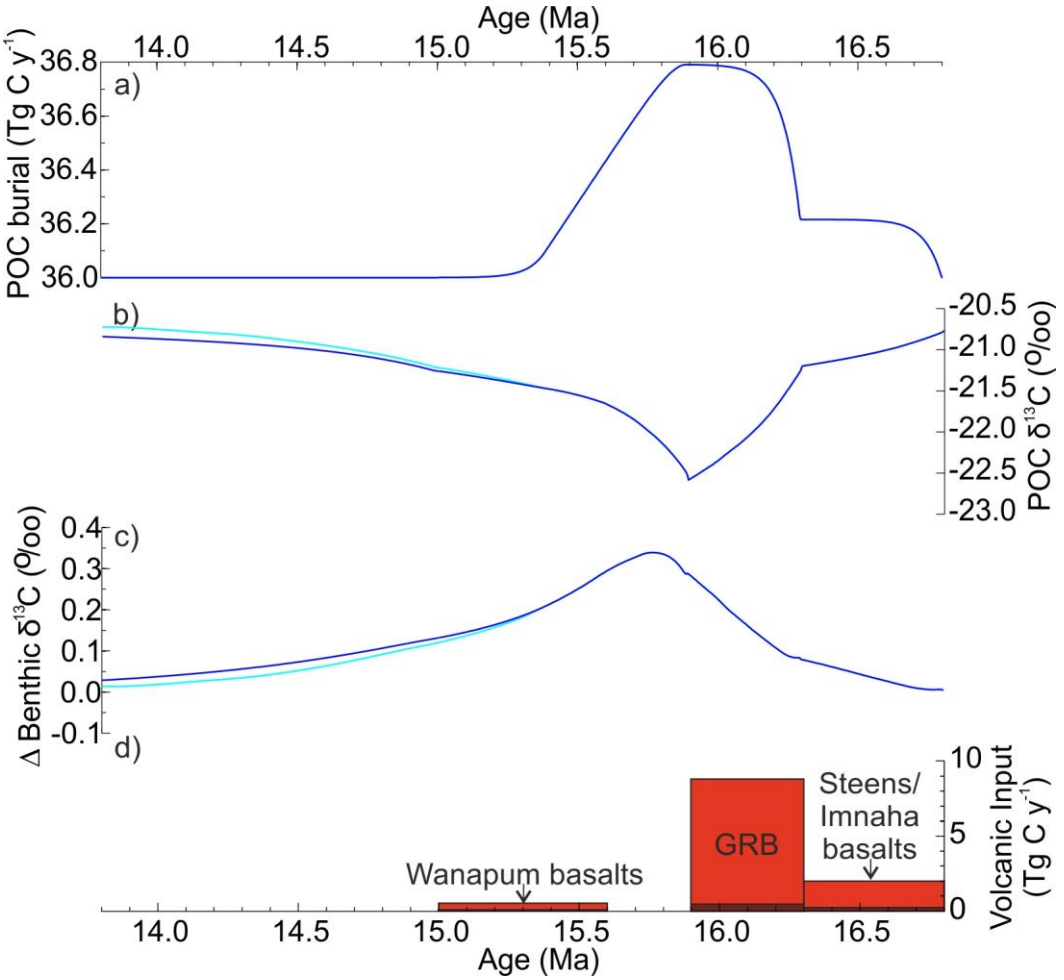

676

677 **Figure 6:** Simulation results in MTW08 of: a) Particulate Organic Carbon (POC) burial
678 rates, b) POC $\delta^{13}C$ and c) change in benthic $\delta^{13}C$ (relative to 16.3 Ma) for our best-fit
679 MTW08 emissions scenario illustrated in panel d) (solid black (dark blue in the web version)
680 line, with additional run with post-CRB glaciation effects shown by the dashed black (light
681 blue in the web version) line). Note the difference between the rate of decrease in POC $\delta^{13}C$
682 and the rate of increase in POC burial.

683 # Tables

Table 1
Estimated liberation rates of silica and phosphorus due to the chemical weathering of the freshly emplaced basalts of the CRB and the estimated resultant increase in baseline silica and phosphorus input to the ocean over 400 ky during the GRB eruptions

Estimate	Chemical weathering rate ($t\ km^{-2}\ y^{-1}$)[a]	Si liberation rate ($mol\ km^{-2}\ y^{-1}$)[b]	P liberation rate ($mol\ km^{-2}\ y^{-1}$)[d]	GRB Si release (% MTW08 baseline)[c]	GRB P release (% MTW08 baseline)[c]
Modern CRB	24.2	$3.0x10^{10}$	$2.4x10^{3}$	0.9	1.3
Mid-Miocene CRB ('fresh' basalt effect)	64.0	$8.0x10^{10}$	$8.9x10^{3}$	2.3	3.5
Resultant surplus[e]	39.8	$5.0x10^{10}$	$5.6x10^{3}$	1.5	2.2

[a] Chemical weathering rates are based on Dessert et al. (2003) and Taylor and Lasaga (1999)
[b] Silica liberation rates based on Dessert et al. (2003)
[c] MTW08 baseline riverine Si and P input listed in Supplementary Information
[d] Phosphorus liberation rates based on scaling Japanese basalt weathering rates (Hartmann and Moosdorf, 2011) to the chemical weathering rate
[e] Surplus P and Si release simulated during the basalt eruptions before decreasing at a constant rate to ~0.1% by 15.1 Ma to represent declining 'freshness' (Taylor and Lasaga, 1999)

684

Table 2
Carbon emission estimates for the entire Columbia River Basalt for different degassing scenarios and sources and the resultant range of the Emission Amplification Factor (EAF) for the CRB

Emission scenario	Emissions for each degassing source (Pg C)					Minimum EAF	Maximum EAF[c]
	Sub-aerial basalts (SAB)	Minimum intrusive magma	Maximum intrusive magma	Minimum total magma	Maximum total magma		
Low degassing[a]	230	230	1240	460	1470	2.0	6.4
High degassing[a]	650	650	3500	1300	4150		
Crust-contaminated[b]	970	970	5220	1940	6190		

[a] Low (0.2% wt. CO_2, 70% efficient) and high (0.5% wt. CO_2, 80% efficient) degassing estimates based on Self et al. (2006) and Shinohara (2008).
[b] Crust-contamination emissions scaled from hypothesised Siberian Traps emissions of Sobolev et al. (2011) by relative volume.
[c] Metamorphic degassing (e.g. Svensen et al., 2004) is also likely to have been significant enough to add to further amplify emissions beyond this value but this impact is currently poorly constrained.

685

686